

Embedded 3D Printing of Thermally-Cured Thermoset Elastomers and the Interdependence of Rheology and Machine Pathing

Maria Stang, Joshua Tashman, Daniel Shiwarski, Humphrey Yang, Lining Yao, and Adam Feinberg*

Thermoset elastomers are widely used high-performance materials due to their thermal stability, chemical resistance, and mechanical properties. However, established casting and molding techniques limit the overall 3D complexity of parts that can be fabricated. Advanced manufacturing methods such as 3D printing have improved design flexibility and reduced development time but have proved challenging using thermally-cured thermosets due to their viscosity, slow gelation kinetics, and high surface tension. To address this, freeform reversible embedding (FRE) 3D printing extrudes thermosets such as polydimethylsiloxane (PDMS) elastomer within a carbomer support bath, but due to the liquid-like state of the prepolymer during extrusion has been limited to hollow structures. Here, FRE printing is significantly improved through rheological modification of PDMS with a thixotropic additive (1.0–10.0 wt.%) that imparts a yield stress (30–120 Pa) to help control filament morphology. Further, print process controls consisting of region-specific slicing, filament retraction, and nonprint travel moves outside of the print to minimize the interaction of the nozzle with previously printed PDMS are implemented. The combined result is the FRE printing of PDMS in complex 3D parts with high fidelity, establishing a 3D printing methodology that can be used broadly with thermally-cured thermoset elastomers and related polymers.

polyether ether ketone (PEEK) can be directly printed into high-performance parts.^[1–5] However, there are still large classes of materials that have been difficult to adapt to 3D printing. For example, thermally-cured thermosets such as epoxies and silicones are widely used in many applications for their combination of mechanical properties, chemical resistance, and thermal stability.^[6] However, these polymers are often two-part systems that must be mixed and then take minutes to hours to crosslink and fully cure. These thermosets remain in a liquid state for a prolonged period and are thus challenging to 3D print with high fidelity because they flow and do not retain their intended geometry. Extrusion-based direct ink writing (DIW) has had success printing thermosets such as epoxies and silicones but typically requires modification of ink composition and rheological properties to make them thixotropic, or that are already thixotropic, to permit printing in air.^[7,8] Additionally, DIW faces


1. Introduction

Three-dimensional (3D) printing has grown as an advanced manufacturing platform, supported by an ever-expanding library of engineering-grade materials with improved properties. This has led to new applications in aerospace, automotive, medical, and other industries where metal powders such as titanium alloys and medical-grade thermoplastics such as

the same geometrical constraints that limit related fused deposition modeling (FDM) type approaches, such as overhangs and free-standing structures that are difficult to print without the use of support material. These constraints on the materials and geometries that can be 3D printed severely limit the complexity of parts that can be fabricated using slow-to-cure liquid prepolymers and soft materials.

Freeform reversible embedding (FRE) 3D printing is a technique that was recently developed to print soft and liquid materials and overcome these challenges.^[9] First described in separate papers by the Feinberg and Angelini groups in 2015, FRE and related embedded 3D printing techniques involve extruding prepolymers into a microgel-based support bath that possesses a yield stress.^[10,11] Unlike typical FDM approaches in which the filament is extruded onto a platform, in FRE the material of choice (often referred to as the ink) is extruded directly into the support bath and held in place until it is cured. The support bath also greatly diminishes the effects of gravity and generally eliminates the need for any additional printed support structures. Despite these advantages, there are still challenges that are unique to the FRE process

M. Stang, J. Tashman, D. Shiwarski, H. Yang, L. Yao, A. Feinberg
Carnegie Mellon University
PA 15213, USA
E-mail: feinberg@andrew.cmu.edu

 The ORCID identification number(s) for the author(s) of this article can be found under <https://doi.org/10.1002/admt.202200984>.

© 2022 The Authors. Advanced Materials Technologies published by Wiley-VCH GmbH. This is an open access article under the terms of the Creative Commons Attribution License, which permits use, distribution and reproduction in any medium, provided the original work is properly cited.

DOI: 10.1002/admt.202200984

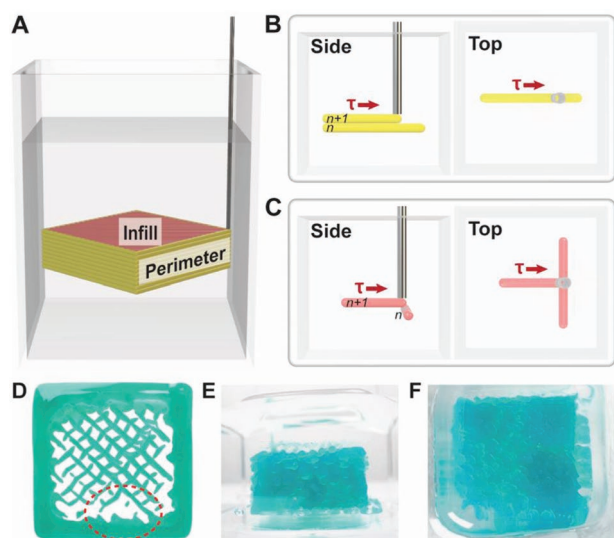


Figure 1. Region-specific forces experienced during FRE 3D printing. A) Render of a calibration cube with infill and perimeter denoted in pink and yellow, respectively. B) In perimeters, filaments are extruded on top of previously deposited filaments. Previous layers experience the downward force of ink as it is extruded as well as shear stress at the interface of layers. This results in minimal perturbation of extruded ink. C) In infill, filaments are often extruded at an angle to the previously deposited filaments. This can result in ink displacement as the nozzle approaches a previous layer. D) Top view of two layers of PDMS with intersecting infill. Red dashed circle highlights the region where infill is disrupted. When attempting to print the full calibration cube, the PDMS coalesces and does not maintain the printed geometry, as seen from the E) side and F) top views in Carbolpol.

when printing liquid prepolymers. Previous work has shown that FRE printing of silicone can be used to produce a range of hollow structures such as tubes that consist primarily of perimeters where each layer is identical, or very similar, to the layer below.^[9,11–15] However, infill patterns where each layer is extruded at an angle to the layer below have been far more difficult because many silicones, epoxies, and other prepolymer inks do not cure instantaneously and instead cure over time or by exposure to external stimuli (e.g., heat, UV light, etc.). These inks are thus often highly deformable after deposition and are susceptible to disruptions from the passing extrusion nozzle during printing. Furthermore, their composition and surface energy can impede fusion (i.e., coalescence of PDMS) unless sufficient contact and applied force between individual filaments is achieved. These unresolved issues have limited the achievable geometries that can be FRE printed and prevented broader adoption in the field.

Here, we sought to improve FRE printing of thermally-cured thermosets by understanding how the rheology, filament morphology, and print pathing of these materials impacts print fidelity and mechanical properties. To do this, we selected polydimethylsiloxane (PDMS) elastomer as a model material due to its widespread use across many industries. Specifically, we used Sylgard 184 because it represents a worst-case scenario for printing due to its Newtonian behavior, making it easy to deform during the print process from the passing extruder nozzle. Previously, we demonstrated that Sylgard 184 could be FRE printed into hollow structures such as five-sided

cubes and developed an expert guided optimization process to improve print fidelity.^[9,13] However, it was still challenging to print objects with infill because each layer being printed would disrupt the easily deformed layer below. To address this, we investigated the causes of this poor print fidelity and then implemented a combination of materials, processing, software, and hardware changes. First, we added a rheological modifier into the PDMS prepolymer to create a yield stress fluid that is more resistant to deformation and thus more capable of maintaining its printed geometry. Second, we quantified filament morphology and deformability in FRE printing during a range of different machine pathing to understand how geometry was being affected. Third, we used this information as inputs for print planning and pathing in slicing software, which takes a computer-aided design (CAD) model and generates the G-code machine pathing for the 3D printer. Importantly, we found that in FRE printing filament cross-sectional geometry and deformability is quite different than in standard FDM prints, which assumes that filaments are flattened during extrusion and do not deform afterward. Our results show that FRE-printed PDMS filaments are highly deformable and dependent on the local surroundings (e.g., region of print, proximity to other filaments, etc.). Since the current slicing software is designed for FDM and not FRE, we used these results to inform and enable improved print process parameter selection, machine pathing, and hardware decisions. Together, this research enables FRE printing of thermally-cured thermoset structures with a high degree of geometric complexity unattainable via other additive manufacturing approaches.

2. Results & Discussion

2.1. Understanding How PDMS Prepolymer Deforms During FRE Printing

FRE printing is directly adapted from extrusion-based 3D printing approaches such as FDM, and therefore is quite similar in terms of the hardware and software used and many of the key process parameters. FDM is primarily used for 3D printing thermoplastic filaments including polylactic acid, acrylonitrile butadiene styrene, and thermoplastic polyurethanes, and has a large industrial user base and has been extensively reviewed.^[16–18] The FRE approach expands the types of materials that can be 3D printed via extrusion, using a support bath to enable the printing of liquid-like materials with rheological properties that differ significantly from those used in FDM. In FDM, thermoplastic filament is transiently heated above its melting point during extrusion and then rapidly cools post-extrusion, becoming rigid. In FRE printing of thermally-cured thermosets, it can take minutes to hours for the material to cure post-extrusion.

The FRE printing of Sylgard 184 PDMS presents an example of the challenge of extruding thermally-cured thermosets because previously printed layers are easily disrupted, with the direction of applied shear stress directly related to the direction of machine pathing. To demonstrate this, we used a calibration cube as the test object with perimeters (the exterior shell) and infill (the interior core) as the two main regions of the print (Figure 1A). Both are important and contribute to the structural

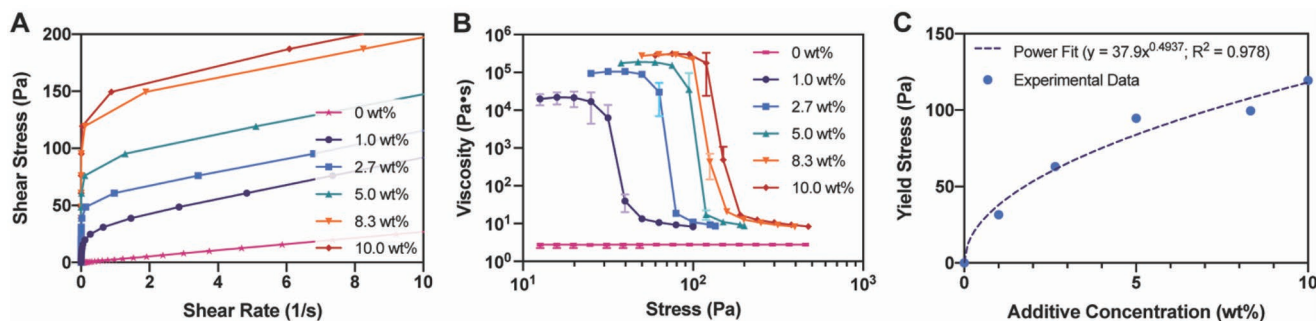


Figure 2. Rheological analysis of PDMS composite inks. A) Stress ramps of Sylgard 184 with increasing concentrations of HS II thixotropic additive from 0 to 10 wt.% demonstrating Bingham pseudoplastic behavior. Sylgard 184 is denoted as 0 wt.%. B) Steady stress sweeps demonstrate an increase in yield stress with increasing HS II thixotropic additive concentration. C) Plot of yield stress versus HS II thixotropic additive concentration, which can be described with a power fit; $R^2 = 0.978$.

integrity of the print, with a greater number of perimeters and higher infill densities typically producing stronger parts. In printing the PDMS calibration cube, it became evident that the forces exerted in the perimeter are fundamentally different than those in the infill. For the perimeters, layer n is first extruded, and layer $n + 1$ is extruded upon it, following an identical or similar path (Figure 1B). Shear stress is generated along the layer interface and in the direction of the filaments in each layer, resulting in minimal material disruption; in this case, any material displacement occurs along the printed path where there is already material. However, for the infill, layer $n + 1$ often traces a path that is at an angle with respect to layer n (Figure 1C). Here, the shear stress can displace material in layer n in the direction of layer $n + 1$, which often results in the displacement of material in layer n away from its printed path and into the surrounding support bath. These effects are especially evident when printing the Sylgard 184 PDMS prepolymer, which exhibits Newtonian behavior and thus flows readily.^[19] When printing the first few layers of a calibration cube, the perimeter stays intact; the filaments within the infill, however, are disrupted due to the interactions with the print nozzle as each layer of infill results in the displacement of material in the previous layer (Figure 1D). Each subsequent layer results in further perturbations of previously extruded ink, making it impossible to maintain the printed geometry. Upon completion of the print, it is apparent that these disruptions compound over time (Figure 1E,F, Video S1, Supporting Information). In the case of FRE-printed PDMS in the aqueous support bath, hydrophobic-hydrophilic mismatch and the resulting interfacial tension also drives coalescence of the PDMS to reduce surface energy, further disrupting print fidelity.^[20,21]

2.2. Use of Thixotropic Additive to Give PDMS a Yield Stress

Based on the results using Sylgard 184 (Figure 1D-E), it was evident that FRE printing with an ink that is Newtonian will always flow when perturbed by the nozzle. To combat this behavior, the rheological modifier HS II thixotropic additive (hereinafter referred to as “HS II”) was added to the PDMS prepolymer to create a yield stress fluid, one that flows only if subjected to a stress above a critical value (known as the yield stress). To minimize changes to the Sylgard 184 PDMS, such as

its high extensibility and low modulus, low concentrations of the HS II at 1.0%–10.0% w/w (1.0, 2.7, 5.0, 8.3, and 10.0% w/w) were added to the PDMS and rheologically characterized. Stress ramps at each concentration revealed that the mixed PDMS and HS II inks were indeed yield stress fluids, as indicated by the nonzero y -intercepts at each concentration (Figure 2A). This rheological profile is desirable for FRE printing because the yield stress must be surpassed to induce flow, making the fluid more capable of resisting deformation upon interactions with the print nozzle.^[22,23] Steady-state stress sweeps were used to determine the yield stress, which is the last value of stress prior to a large drop in viscosity, and confirmed that yield stress increased with HS II concentration (Figure 2B). This behavior can be described with a power law (Figure 2C), where the yield stress plateaus at greater HS II concentrations. To minimize potential changes to the unmodified PDMS properties, a concentration of 2.7% (w/w) HS II was selected for all prints because it imparted a yield stress while still being easily extruded from the nozzle. Extrusion became increasingly difficult with higher HS II concentrations.

2.3. Filament Cross-Section Morphology in FRE Deviates from that in FDM

Another significant factor that impacts print fidelity is filament morphology, as this directly relates to the geometric calculations made in the machine pathing to create a 3D object.^[22] To date, most extrusion-based 3D printing, including FRE, has used established FDM slicing software, which assumes that 1) filaments are flattened onto the print platform during extrusion, with a thin and wide elliptical cross-section, and 2) filaments do not deform after extrusion (Figure 3A,B).^[24–26] This expectation holds for FDM because the thermoplastic filament is melted, extruded, and flattened against the layer below it, where it subsequently rapidly cools and solidifies. In FRE, the thermally-cured ink is slow to cure and extruded within a yield-stress support bath instead of onto a build platform. The result is a radically different filament morphology, with an elliptical cross-section that is taller than it is wide (Figure 3A,C). We investigated this further by varying several print parameters using a window frame test model with single filaments printed across the center to facilitate cross-sectional

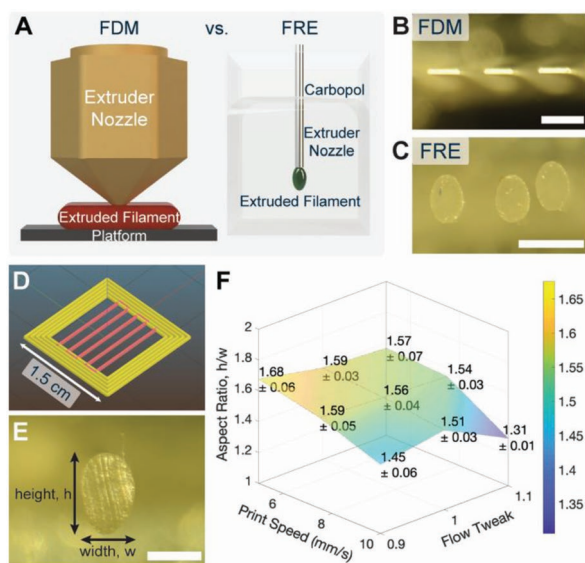


Figure 3. Investigation of filament cross-sectional morphology. A) Schematic of filament cross-sections during printing in FDM and FRE. Filament morphologies differ between B) FDM and C) FRE. Scale bars: 1 mm. (D) Frame model used to analyze aspect ratio of single filaments. E) Cross-section of filament printed at 5 mm/s and a flow tweak of 1. Scale bar: 0.5 mm. F) Aspect ratio is consistently greater than 1 over a range of print speeds (5–10 mm s⁻¹) and flow tweaks (0.9–1.1).

analysis (Figure 3D). The window frame was sectioned through the middle and the aspect ratio of each filament was quantified by dividing the height by the width (Figure 3E). Constructs were printed at three different print speeds of 5, 7.5, and 10 mm s⁻¹ and flow tweaks of 0.9, 1.0, and 1.1 to determine the sensitivity of the aspect ratio to these parameters. Flow tweak (also known as the extrusion multiplier) is a parameter in the slicing software used to fine tune material flow rate from the ideal flow rate calculated by the software. This can be used to effectively change how much material is deposited, where values <1.0 will result in under-extrusion and values >1.0 will result in over-extrusion. Print speed dictates print time and impacts fidelity, especially when using higher-viscosity inks, where the syringe pump extruder may have difficulty delivering the intended amount of ink in the time given. Image analysis revealed that across the entire parameter space, the aspect ratio was greater than one, and for a given flow tweak, increasing the print speed decreased the aspect ratio (Figure 3F). This morphology suggests that there is an area of low pressure directly trailing the print nozzle within the temporarily fluidized support bath, and the PDMS ink fills this space until it is immobilized by the resolidified support bath.^[22,27,28] These results establish that under typical print speeds and flow tweaks, the filament morphology of suspended filaments in FRE have an aspect ratio of ≈1.5, which deviates notably from the aspect ratio of ≈0.25 assumed in standard FDM slicing software. This difference can result in sub-optimal G-code generation for a construct and produce print defects like under- or over-extrusion, resulting in poor print fidelity. The dependence of print fidelity in FRE on print parameters as well as ink and support bath rheology has been demonstrated in the literature and corroborates the results here.^[22,29]

2.4. PDMS Ink Deformability and Morphology During and After Printing are Dependent on Local Interactions

Material deformability post-extrusion is a key factor that needs to be understood because the PDMS with the HS II thixotropic additive has a >4 h cure time and yield-stress behavior during this period. The interactions between adjacent filaments within and between layers are of interest because this will inform optimal filament placement (packing) during the generation of the G-code.^[22] However, as already noted, the physical interactions between extrusions are different for perimeter versus infill (Figure 1B,C). First, to determine how filaments in perimeters deform, hollow cylinders with 2, 3, and 4 layers were printed and sectioned in half (Figure 4A). The original Z step (Z₀), which was equal to the default layer height generated by the slicing software was adjusted to 50, 60, 70, 80, and 90% of Z₀. Evaluation of the filament cross-sections revealed that a Z step equal to 60% of Z₀ was sufficient to achieve fusion between filaments. When printing 2 layers, the interface between the layers became flattened due to the deformation of the PDMS filaments; however, the bottom region of the bottom filament and the top region of the top filament remained rounded, similar to single filament morphology (Figure 4B). In contrast, when printing three or more layers, filaments in intermediate layers deformed on both the top and bottom, adopting a morphology similar to thermoplastic filaments in FDM. Thus, for perimeters the filament morphology of the PDMS ink is comparable to what is expected in FDM printing, suggesting that slicing software can provide appropriate G-code.

The situation for infill is different, and to investigate this filament deformability in more detail, the window frame model in Figure 3D was modified to possess a single layer, where infill density was varied from 10% to 90% to control lateral filament spacing. At 40% infill, where the filaments were widely spaced, the aspect ratio was ≈1.4 (Figure 4C), similar to the single filament experiments. However, stepwise increases showed that in the range of 60%–70% infill density, the aspect ratio increased, and filaments began to be deformed due to the proximity of adjacent filaments being printed (Figure 4D). At these higher infill densities, the nozzle is close enough to already printed filaments in the same layer to displace them laterally during printing. Next, we printed the window frame model with both increasing infill densities (30%, 50%, and 70%) and increasing layers (2, 3, 4, and five layers). Low density infill of 30% appeared similar to the perimeter printing due to relatively large lateral spacing between filaments. However, at higher infill densities, lateral filaments were packed closer to one another, resulting in deformation vertically in Z (Figure 4E). At high infill densities (seen at 70% for constructs with more than two layers), this vertical filament deformation translated into crowning, a print defect (as indicated by asterisks) where there is an undesirable excess of material in a region of a print above the layer being printed. Thus, although the Z step needed to be adjusted for perimeters to achieve fusion, this was not necessary for 3D constructs with infill. This is possibly due to an increasing frequency of interactions with the print nozzle that can encourage fusion. Therefore, for all subsequent prints, the Z step was not modified in the G-code.

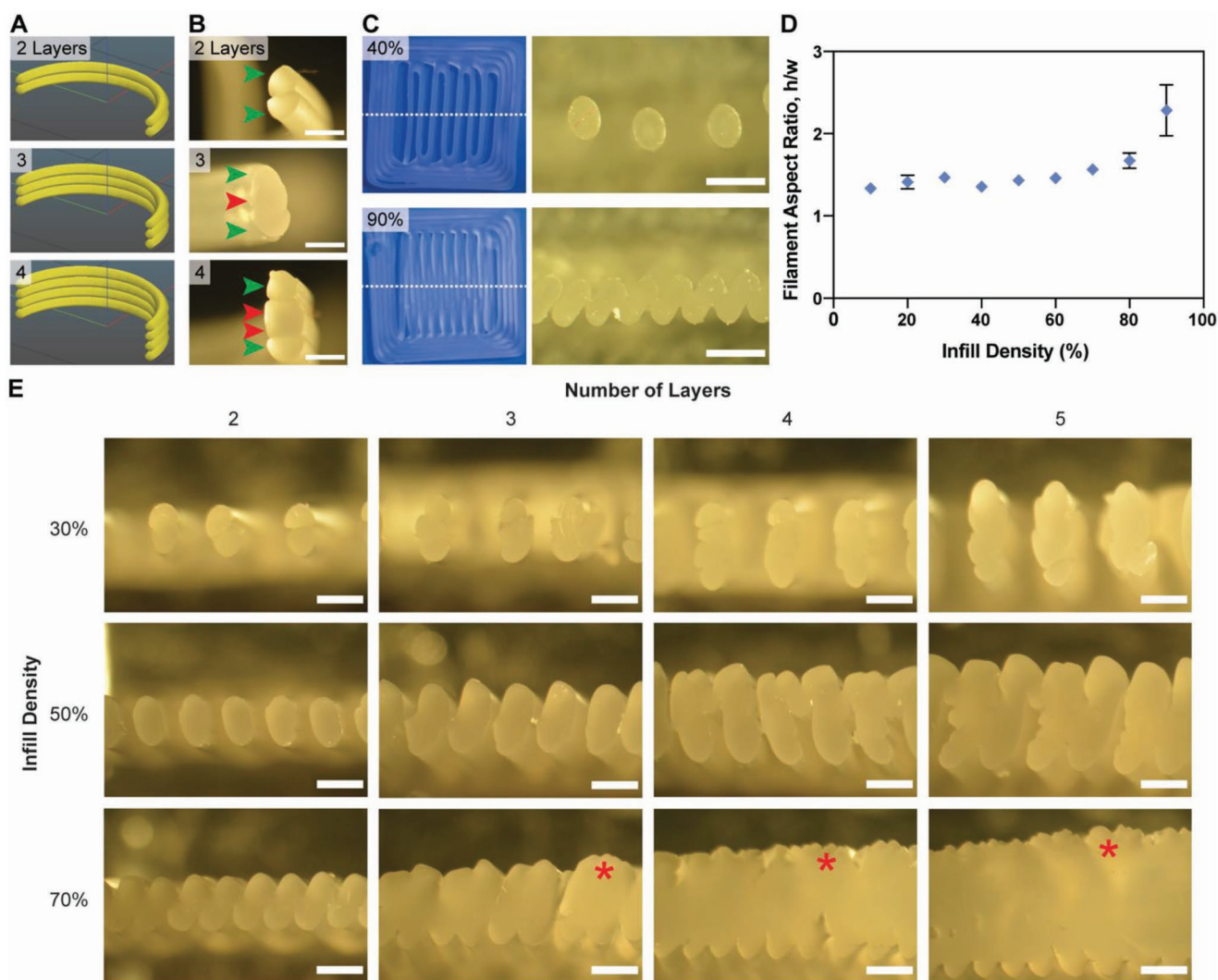


Figure 4. Investigation of filament morphology for perimeters and infill. A) Machine pathing for cylinders with 2, 3, and 4 layers. B) Cross-sections of stacked filaments with 2, 3, and 4 layers exhibit 2 distinct morphologies: rounded and flattened, as indicated by the green and red arrowheads, respectively. C) Frame model used to examine filament morphology as a function of infill density. Printed constructs are cut at the dashed white line, and cross-sections are examined with a stereomicroscope. Top and cross-sectional views of a single layer of filaments at 40% and 90% infill densities. Filament elongation is especially exacerbated at high infill densities. D) Plot of aspect ratio versus infill density shows an increase in aspect ratio above $\approx 60\%$ infill density. E) Filament cross-sections over a range of infill densities and number of layers. Asterisks denote regions of crowning. Scale bars: 1 mm.

Next, we applied this understanding of filament deformation for perimeter and infill by printing a solid 3D cube using a range of print settings (Figure 5). As previously noted, when printing the unmodified PDMS prepolymer, there was extensive coalescence throughout the entire cube structure (Video S1, Supporting Information). Despite this, the support bath maintained the approximate shape of the cube, but upon Carbopol dissolution and print removal the cube fell apart leaving behind chunks of cured PDMS (Figure 5, top row). This demonstrates that when using PDMS inks that have Newtonian rheology and cure slowly, it is not possible to print the 3D cube, regardless of print settings. However, by incorporating the HS II thixotropic additive (at 2.7% w/w) a major improvement in print fidelity was achieved, and upon release from the support bath, layers were fused together and the cube remained intact. Closer inspection revealed that the print had numerous defects,

such as crowning (denoted by red asterisks) and inconsistent fusion (denoted by black asterisks, Figure 5, middle row). These defects were due in part to material displaced vertically into adjacent layers where it could then be shifted by the print nozzle during travel moves. For example, upon completion of a layer, the print nozzle rose in *Z* and dragged ink from one corner of the cube to the other as it transitioned to printing the next layer (Video S2, Supporting Information). This highlights the difficulties of printing with a deformable ink in an embedded printing system, where forces applied by the nozzle during printing are required for contact between adjacent filaments, but these forces can also disrupt the ink and displace it from its intended location. To address this, machine pathing is modified to have travel moves (movements that do not involve ink extrusion and thus play no role in fusion) take place outside of the body of the print to minimize material displacement.

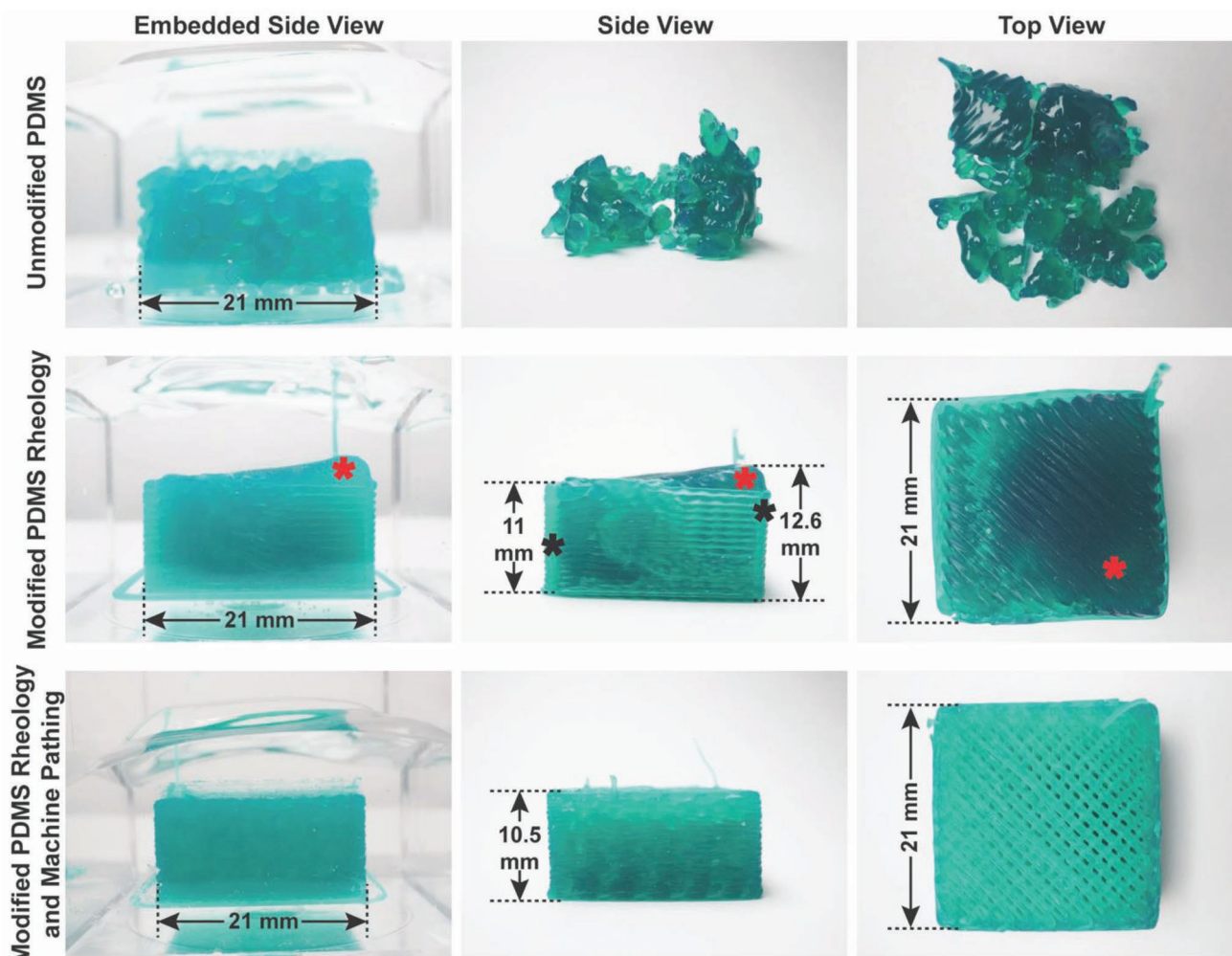


Figure 5. Optimization of FFF printing of a calibration cube via modification of PDMS rheology and machine pathing. Printing unmodified PDMS results in the coalescence of PDMS. Disruption of previously printed layers manifests in droplets of PDMS. When PDMS rheology is modified through the addition of HS II thixotropic additive, it is possible to produce the calibration print, but it has numerous print defects, such as crowning (denoted by red asterisks) and areas of inconsistent fusion (black asterisks). Poor fusion is obtained in some areas between the infill and perimeter. Upon modifying the machine pathing, a calibration cube is printed with much improved fidelity as assessed by the external surface.

Further, infill densities of 90% or less are generally sufficient to prevent crowning when the extrusion width is 50% of the layer height. In making these changes, a calibration cube with good interlayer fusion was printed (Figure 5, bottom row and Video S3, Supporting Information). These modifications were used to inform print parameter selection and machine pathing in all future prints.

2.5. The Impact of Pathing and PDMS Ink Composition on Mechanical Properties

An important consideration is whether the modification made by adding HS II thixotropic additive to the PDMS ink impacted filament fusion and mechanical properties. To determine the impact of the HS II thixotropic additive, three PDMS formulations with 0%, 1.0%, and 2.7% w/w HS II were cast into sheets and laser cut into dog bones for uniaxial tensile

testing (Figure 6A). These tests revealed that elastic modulus decreased with increasing HS II concentration, which suggests the possibility that the HS II acts as a plasticizer and decreases crosslink density in the PDMS network (Figures 6B,C,D).^[30] Next, three infill patterns were selected for printing: 1) cubic, which is a 3D infill pattern consisting of stacked and tilted cubes; 2) aligned rectilinear, with filaments in the direction of uniaxial tensile loading (denoted as “parallel”); and 3) aligned rectilinear, with filaments perpendicular to the direction of uniaxial tensile loading (denoted as “perpendicular”) (Figures 6E,F). Rectilinear infill patterns are commonly used in 3D prints and were chosen to determine how filament directionality impacts mechanical properties. Cubic infill was chosen because it can be used for functional 3D prints that require strength in multiple directions.^[31] For mechanical tests, the specimens were sliced with a one-line shell at the perimeter of each layer. We made two changes to the infill lines to improve the specimen’s quality. Due to the printed filament morphology, the infill lines

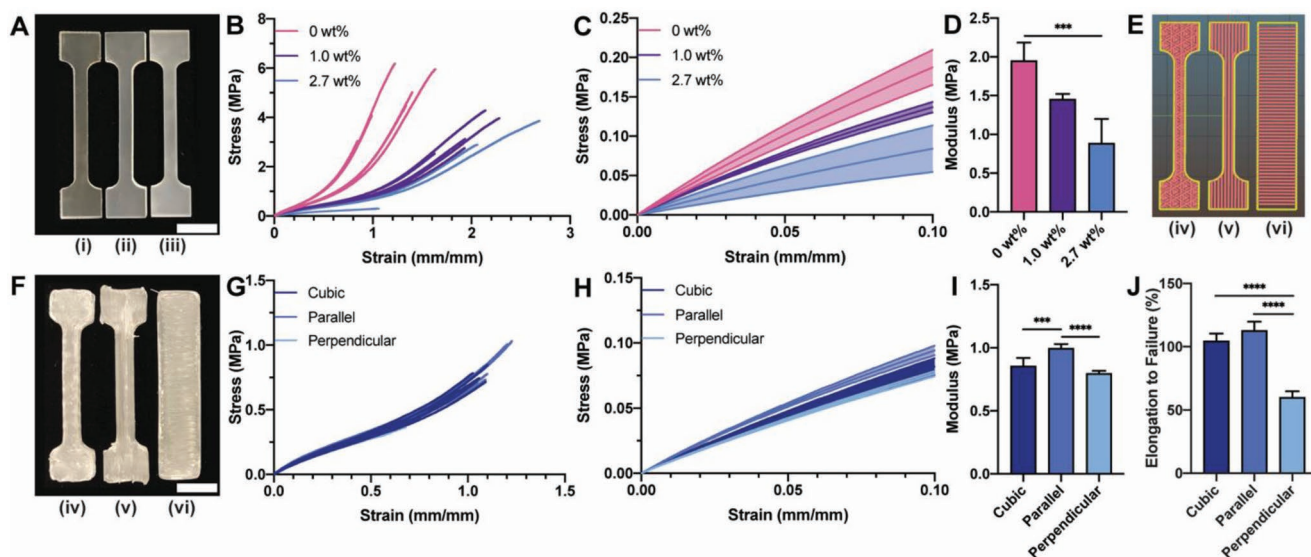


Figure 6. Mechanical properties of casted and printed constructs. A) Top view of casted tensile testing specimens at (i) 0 wt.%, (ii) 1.0 wt.%, and (iii) 2.7 wt.% HS II thixotropic additive. Scale bar: 1 cm. B) Individual stress-strain curves for three different the PDMS formulations as a function of weight percent of HS II thixotropic additive ($n = 6$). C) Stress-strain curves for three the PDMS formulations ($n = 6$) at 0%–10% strain, each curve shows mean and standard deviation. D) Elastic modulus of three the different PDMS formulations (Kruskall-Wallis test with post-hoc Dunn’s multiple comparisons test, *** indicates $p < 0.001$). E) Machine pathing for tensile testing specimens with (iv) cubic, (v) aligned rectilinear, fill angle = 0° (denoted as “parallel”), and (vi) aligned rectilinear, fill angle = 90° (denoted as “perpendicular”) infill patterns. F) Top view of printed (left to right: cubic, parallel, and perpendicular infill patterns) tensile testing specimens. Scale bar: 1 cm. G) Stress-strain curves for three different infill patterns ($n = 6$). H) Stress-strain curves for three different infill patterns ($n = 6$) at 0%–10% strain, each curve shows mean and standard deviation. I) Elastic modulus of printed tensile test specimens as a function of infill pattern for the at 2.7 wt.% HS II thixotropic additive (one-way ANOVA and post-hoc Tukey’s test, *** indicates $p < 0.001$, **** indicates $p < 0.0001$). J) Elongation to failure as a function of infill pattern (one-way ANOVA and post-hoc Tukey’s test, **** indicates $p < 0.0001$).

were offset by half of the infill line spacing at alternate layers. This modification enabled the elliptical infill lines to stack up densely (i.e., circular packing pattern) into a solid cross-section approximating the casted samples. Additionally, the infill lines were extended by the printing nozzle’s diameter at both ends to make sure the infill lines fused well with the perimeter filaments. Furthermore, perpendicular specimens were printed as rectangular strips as opposed to dog bones due to voids present at the neck when the model was input into slicing software. Tensile testing showed that parallel constructs had a significantly greater effective elastic modulus than the other two constructs (Figure 6G,H,I). Further, parallel and cubic constructs had a greater elongation to failure as compared to perpendicular constructs. The impact of filament directionality on mechanical properties is consistent with conventional FDM, where constructs are weaker between layers (Figure 6J).^[32]

2.6. Improving Fidelity of Complex Parts Through Modified Machine Pathing, Print Process Parameters, and Stronger Hardware

Finally, we sought to demonstrate additional approaches to improve the fidelity of PDMS prints through software and hardware modifications that impact the print process. First, a hollow sphere was printed because the curvature and overhangs present a major challenge in 3D printing. While the layers on the bottom fused well using default settings, there was layer separation present in the top quarter of the sphere (Figure 7A).

To enhance layer fusion, multiple modifications to printing were made. First, the G-code was modified for different layers, increasing from 4 to 6 perimeters for the top 3 mm of the sphere, along with an increase in flow tweak from 1.0 to 1.25. The addition of extra perimeters as well as a higher flow tweak (i.e., flow rate) resulted in a greater amount of ink extruded, which improved fusion. Second, a smaller needle (ID = $305 \mu\text{m}$) was used to decrease the layer height and smooth out the surface of the entire sphere. Together, these changes resulted in fusion through all layers of the sphere and highlight the importance of using advanced features in slicers such as layer modifiers. Next, an auxetic lattice was selected to demonstrate the importance of retraction and nonprint travel moves (Figure 7B). Retraction is a printing command that pulls material back into the nozzle to prevent unwanted material from oozing out of the nozzle, which can result in stringing artifacts. Also, a lift command was implemented with retraction during travel moves, which causes the extruder nozzle to lift a specified distance in Z above the layer that is currently being printed. This ensures that the nozzle will not drag material from one region of the print to another; this is especially important in FRE where vertical filament elongation in Z (as demonstrated in Figure 4) can displace material upward. Printing the auxetic lattice using standard settings resulted in frequent stringing, especially on the outer perimeter of the construct. These most likely result from ink oozing out of the nozzle during travel moves as well as ink displacement by the nozzle. By implementing retraction and lift commands, stringing events were greatly reduced while maintaining interlayer fusion. The mechanical integrity of the construct was

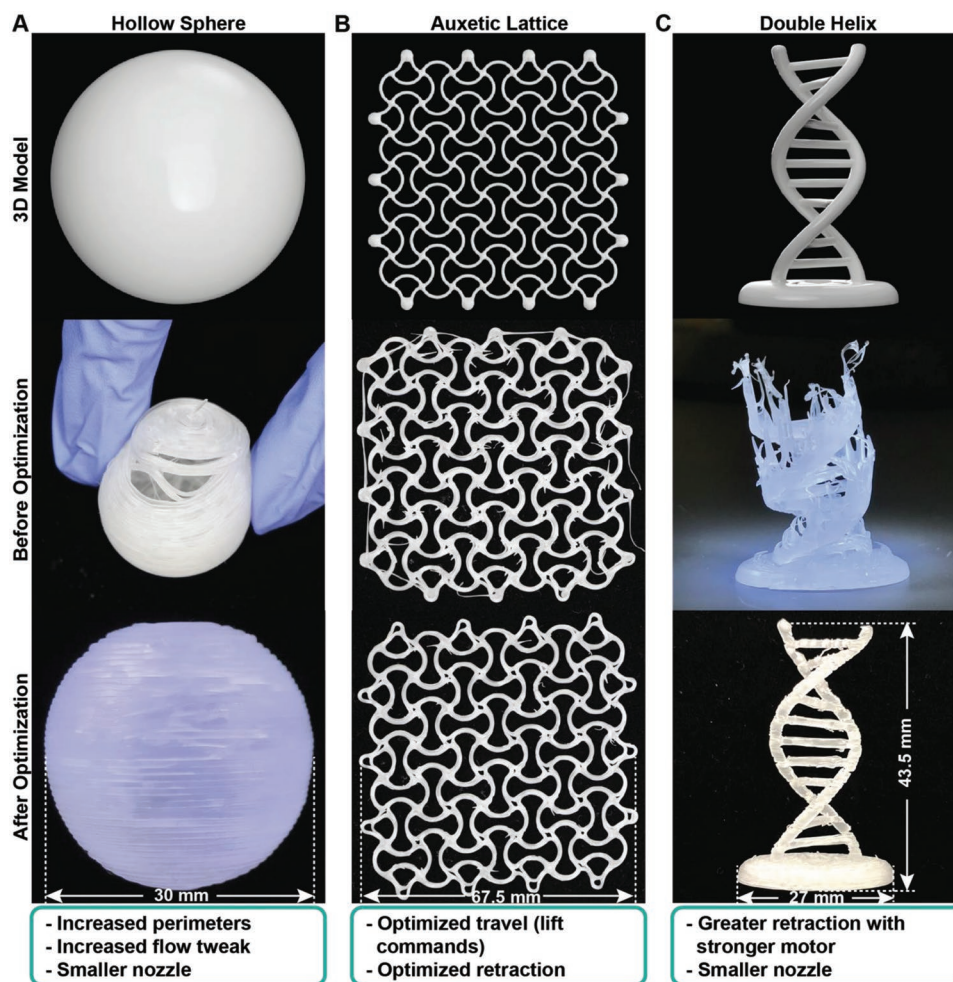


Figure 7. Optimization of machine pathing and utilization of upgraded hardware demonstrate the versatility of the FRE printing platform. A) Generating separate machine pathing (increasing the number of perimeters, flow rate) for different regions of a print enables the construction of a hollow sphere. B) Implementing retraction and lift travel moves enables the construction of an auxetic lattice. C) Utilizing a smaller nozzle size and stronger motor enables greater retraction and thus the construction of a right-handed double helix.

confirmed by stretching the lattice to show the negative Poisson's ratio (Video S4, Supporting Information). Last, a DNA-like double helix ladder was selected because it has fine features, overhangs, and unsupported horizontal sections that are difficult to print via extrusion-based methods (Figure 7C). Initial prints failed, with vertical stringing during nozzle lifts for retraction that caused major defects. This was due, in part, to the high viscosity of the modified PDMS ink and the frequent retractions required for this specific print. It was determined from empirical observation of the printing process that the original stepper motor could not provide sufficient force to retract the PDMS in the specified time. To address this, a larger stepper motor that had more torque was used on the extruder (Figure S1, Supporting Information). This hardware change also enabled the use of a smaller nozzle (ID = 406 μm). The result was a major improvement in print fidelity producing a double helix with a solid base, small features, and few stringing events. These prints demonstrate the importance of layer-specific G-code, retraction, nonprint travel moves, and high-performance hardware that is capable of extruding thixotropic, viscous fluids.

3. Conclusion

It is clear that many factors influence the success of printing liquid prepolymers using FRE. Rheological modification of prepolymers can be leveraged to create yield stress fluids that are more capable of maintaining their printed geometries. This alone does not lead to print success; additionally, intelligent machine pathing and careful selection of print parameters are necessary. Specifically, interactions between the print nozzle and extruded filament should be minimized to prevent filament distortion. Travel moves should take place outside the body of the print, and retraction should be employed to diminish stringing artifacts. A modular approach to machine pathing may be needed to achieve printed constructs with the highest fidelity. Finally, a robust printing platform with hardware capable of extruding thixotropic, viscous fluids is required. We expect that the findings provided herein can also be extended to other thermally-cured thermosets, greatly expanding our capabilities of printing slow-to-cure prepolymer systems.

4. Experimental Section

Preparation of Carbopol Support Bath: A 0.2% (w/v) Carbopol support bath was prepared according to published methods.^[9,13,15] Briefly, 4 g of Carbopol 940 (Lubrizol) were slowly added to 2 L of distilled water and mixed with a KitchenAid mixer for 15 min. Sodium hydroxide (1.0 N) (EMD Millipore) was then used to neutralize the bath to a pH of 7.0–7.1, inducing immediate gelling. The bath was mixed for an additional 5 min to ensure homogeneity. Prior to 3D printing, Carbopol gel was mixed for 2 min at 2000 RPM followed by 2 min of degassing at 2000 RPM in a planetary centrifugal mixer (Thinky).

Preparation of PDMS Composite Inks: Sylgard 184 elastomer (Dow Silicones Corporation) was prepared per manufacturer's directions by mixing 10 parts base to 1 part curing agent in a planetary centrifugal mixer (Thinky) for 2 min at 2000 RPM followed by 2 min of degassing at 2000 RPM. Five different PDMS composite inks were created by mixing HS II thixotropic additive (Dow Silicones Corporation) at 1.0, 2.7, 5.0, 8.3, and 10.0% (w/w) with Sylgard 184 using the same mixing and degassing cycle. Silc Pig silicone color pigments (Smooth-On, Inc.) were used for contrast and incorporated into the PDMS prepolymer with HS II thixotropic additive prior to mixing.

Rheology: To measure the rheological properties of the PDMS composite inks, each formulation was loaded onto a rheometer (Discovery Hybrid Rheometer [DHR-2], TA Instruments) equipped with a 40 mm diameter, 1° cone. Stress ramps were conducted from 0.1–1000 Pa to obtain flow curves. Steady state stress sweeps were conducted over a range of 5–500 Pa for yield stress analysis; yield stress values were designated as the last data point before a significant drop in viscosity. These values were fit to a power curve in MATLAB. All curves were plotted in GraphPad Prism 8.4.2.

FRE 3D Printing: 3D printing of PDMS composite inks was performed on three printers: 1) a Lulzbot Mini 2 modified with a custom-designed syringe pump extruder (Replistruder 4)^[33] (Figure S1A, Supporting Information) was used for prints in Figures 1, 5, and 6; 2) a FlashForge Finder Pro modified with a Replistruder 4 was used for prints in Figures 3 and 4; and 3) a MakerGear M2 3D Printer (Rev. E.) modified with a newly designed syringe pump specifically created for high-viscosity, thixotropic materials (Replistruder 4 High Viscosity) (Figure S1B, Supporting Information) was used for prints in Figure 7. The 3D models for the calibration cube, hollow sphere, auxetic lattice, and double helix were obtained from the Thingiverse database (<https://www.thingiverse.com>). All STL files were processed by Slic3r (<https://slic3r.org>) software. Custom G-code was created for each print region of interest (using modifiers in Slic3r) and subsequently merging the code in a text editor (Sublime Text). For filament morphology and deformability investigations, a custom MATLAB script was used to adjust the Z step to 60% of the layer height to obtain fusion. Prior to printing, PDMS composite inks were transferred into a 5.0 mL gastight glass syringe (Hamilton) and mounted into the syringe pump. Stainless steel dispensing needles 1 inch long (Jensen Global) were used with either a 635 μm or 406 μm ID needle, unless otherwise specified. Carbopol was prepared and added to acrylic containers large enough to house the printed constructs. The container was secured to the print platform with a thin layer of vacuum grease. The needle was positioned in the center of the container and lowered in the support, leaving a small gap between the needle and the container bottom. Upon print completion, the print container was removed from the print platform and the PDMS was allowed to cure overnight in an oven at 65 °C. After curing, sodium chloride was sprinkled on the Carbopol support to induce liquefaction, enabling print removal.

Replistruder 4 and Replistruder 4 High Viscosity: The Replistruder 4 is a fixed displacement syringe pump with a design optimized for extrusion-based printing of soft materials.^[33] This design incorporates a single lead screw and a cantilevered carriage that pushes on a syringe plunger to extrude material. For many soft materials with low viscosities the Replistruder 4 is capable of high resolution and fidelity printing using small diameter needle tips. For higher viscosity materials, however, the cantilevered geometry can affect print capabilities, limiting the smallest diameter needle tip that can be used. To overcome this a more rigid

design, the Replistruder 4 High Viscosity, was created. This design has increased rigidity and incorporates 2 leadscrews with a carriage that straddles the syringe plunger to eliminate the cantilever geometry. In conjunction with a larger stepper motor, these changes allow for printing higher viscosity soft materials with smaller diameter needle tips.

Analysis of FRE Printed PDMS Structures: To evaluate filament and print morphology, a window frame model was printed over a range of print speeds (5–10 mm s^{-1}), flow tweaks (0.9–1.1), infill densities (10%–90%), and print heights (1–5 print layers). Additionally, hollow cylinders were printed with 2–4 layers. These constructs were cut through the middle, and the filament cross-sections were examined on a stereomicroscope (Nikon SMZ1500). Aspect ratio was analyzed by measuring the height and width of each filament using ImageJ (<https://imagej.nih.gov/>) software. A surface plot of aspect ratio as a function of print speed and flow tweak was generated in MATLAB, and the aspect ratio as a function of infill density was plotted in GraphPad Prism 8.4.2.

Mechanical Properties: Three PDMS formulations (0 wt.%, 1.0 wt.%, and 2.7 wt.% HS II) were cast into 150 mm diameter Petri dishes to a thickness of ≈ 3 mm and allowed to partially cure at room temperature overnight. Complete curing was obtained by placing the PDMS formulations in a 65 °C oven for 4 h. Tensile bar strips were laser cut with a Rabbit laser cutter (model: RL-80-1290, Rabbit Laser USA). Additionally, tensile test strips were FRE 3D printed at 2.7 wt.% HS II with three infill types (cubic; aligned rectilinear, fill angle = 0°; aligned rectilinear, 90°). Uniaxial tensile testing was conducted on all samples using an Instron 5943, with a total of 6 samples per condition. Samples were stretched at a rate of 2.00 mm min^{-1} until failure. The modulus was determined from a simple linear regression of the stress-strain curves from 0–10%. Statistical analyses were performed using GraphPad Prism 8.4.2. Kruskal-Wallis test with post-hoc Dunn's multiple comparisons test was used to evaluate the significance of elastic moduli of casted constructs. One-way ANOVA and post-hoc Tukey's tests were used to evaluate the significance of elastic moduli and elongation to failure of printed constructs.

Supporting Information

Supporting Information is available from the Wiley Online Library or from the author.

Acknowledgements

This material was based upon work supported by the National Science Foundation Graduate Research Fellowship Program under Grant No. DGE 1745016. Any opinions, findings, conclusions, or recommendations expressed in this material are those of the author(s) and do not necessarily reflect the views of the National Science Foundation. This research was also supported by the National Heart, Lung, and Blood Institute of the National Institutes of Health (F32HL142229, F30HL154728, K99HL155777). This research was also supported by the CMU Manufacturing Futures Initiative, made possible by the Richard King Mellon Foundation. The authors would like to acknowledge Bradford and Diane Smith for their generous support through the Bradford and Diane Smith Graduate Fellowship. The authors would like to thank Connor Valentine and Professor Lynn Walker for their guidance and training on rheological methods and analyses. The authors would also like to thank Dr. Rachelle Palchesko for her guidance and training on tensile testing.

Conflict of Interest

The authors declare the following competing financial interest(s): A.W.F. has an equity stake in FluidForm Inc., which is a startup company commercializing FRE 3D printing. FRE 3D printing is the subject of patent protection including U.S. Patent 10,150,258 and others owned by Carnegie Mellon University.

Data Availability Statement

The data that support the findings of this study are available from the corresponding author upon reasonable request.

Keywords

3D printing, freeform reversible embedding, polydimethylsiloxane, rheology, machine pathing

Received: June 16, 2022
Revised: October 2, 2022
Published online:

- [1] T. D. Ngo, A. Kashani, G. Imbalzano, K. T. Q. Nguyen, D. Hui, *Composites, Part B* **2018**, *143*, 172.
- [2] H. Attar, M. Calin, L. C. Zhang, S. Scudino, J. Eckert, *Mater. Sci. Eng., A* **2014**, *593*, 170.
- [3] X. P. Tan, Y. J. Tan, C. S. L. Chow, S. B. Tor, W. Y. Yeong, *Mater. Sci. Eng., C* **2017**, *76*, 1328.
- [4] S. Singh, C. Prakash, S. Ramakrishna, *Eur. Polym. J.* **2019**, *114*, 234.
- [5] P. Honigmann, N. Sharma, B. Okolo, U. Popp, B. Msallem, F. M. Thieringer, *Biomed Res. Int.* **2018**, *2018*, 4520636.
- [6] M. A. A. AlMaadeed, D. Ponnamma, A. A. El-Samak, in *Polymer Science and Innovative Applications* (Eds: M. A. A. AlMaadeed, D. Ponnamma, M. A. Carignano), Elsevier, New York **2020**, Ch. 1.
- [7] J. A. Lewis, *Adv. Funct. Mater.* **2006**, *16*, 2193.
- [8] V. Ozbolat, M. Dey, B. Ayan, A. Povilianskas, M. C. Demirel, I. T. Ozbolat, *ACS Biomater. Sci. Eng.* **2018**, *4*, 682.
- [9] T. J. Hinton, A. Hudson, K. Pusch, A. Lee, A. W. Feinberg, *ACS Biomater. Sci. Eng.* **2016**, *2*, 1781.
- [10] T. J. Hinton, Q. Jallerat, R. N. Palchesko, J. H. Park, M. S. Grodzicki, H.-J. Shue, M. H. Ramadan, A. R. Hudson, A. W. Feinberg, *Sci. Adv.* **2015**, *1*, e1500758.
- [11] T. Bhattacharjee, S. M. Zehnder, K. G. Rowe, S. Jain, R. M. Nixon, W. G. Sawyer, T. E. Angelini, *Sci. Adv.* **2015**, *1*, e1500655.
- [12] C. S. O'Bryan, T. Bhattacharjee, S. Hart, C. P. Kabb, K. D. Schulze, I. Chilakala, B. S. Sumerlin, W. G. Sawyer, T. E. Angelini, *Sci. Adv.* **2017**, *3*, e1602800.
- [13] S. Abdollahi, A. Davis, J. H. Miller, A. W. Feinberg, *PLoS One* **2018**, *13*, e0194890.
- [14] A. Menon, B. Póczos, A. W. Feinberg, N. R. Washburn, *3D Print. Addit. Manuf.* **2019**, *6*, 181.
- [15] S. Abdollahi, E. J. Markvicka, C. Majidi, A. W. Feinberg, *Adv. Healthcare Mater.* **2020**, *1901735*, 1901735.
- [16] O. A. Mohamed, S. H. Masood, J. L. Bhowmik, *Adv. Manuf.* **2015**, *3*, 42.
- [17] V. Dhinakaran, K. P. M. Kumar, P. M. B. Ram, M. Ravichandran, M. Vinayagamoorthy, *Mater Today Proc* **2020**, *27*, 752.
- [18] B. Shaqour, M. Abuabiah, S. Abdel-Fattah, A. Juaidi, R. Abdallah, W. Abuzaina, M. Qarout, B. Verleije, P. Cos, *Int J Adv Manuf Technol* **2021**, *114*, 1279.
- [19] F. Schneider, J. Draheim, R. Kamberger, U. Wallrabe, *Sens. Actuators, A* **2009**, *151*, 95.
- [20] D. J. Shiwarski, A. R. Hudson, J. W. Tashman, A. W. Feinberg, *APL Bioeng* **2021**, *5*, 010904.
- [21] W. Hua, K. Mitchell, L. Raymond, B. Godina, D. Zhao, W. Zhou, Y. Jin, *ACS Biomater. Sci. Eng.* **2021**, *7*, 4736.
- [22] L. M. Friedrich, J. E. Seppala, *Soft Matter* **2021**, *17*, 8027.
- [23] E. J. Courtial, C. Perrinet, A. Colly, D. Mariot, J. M. Frances, R. Fulchiron, C. Marquette, *Addit. Manuf.* **2019**, *28*, 50.
- [24] P. Ravi, *3D Print Med* **2020**, *6*, 10.
- [25] M. Hebda, C. McIlroy, B. Whiteside, F. Caton-Rose, P. Coates, *Addit. Manuf.* **2019**, *27*, 99.
- [26] R. Comminal, M. P. Serdeczny, D. B. Pedersen, J. Spangenberg, *Addit. Manuf.* **2018**, *20*, 68.
- [27] B. S. Bixler, in *Handbook of Sports Medicine and Science: Swimming* (Eds.: J. M. Stager, D. A. Tanner), Blackwell Science Ltd, Oxford, UK **2005**, Ch. 4.
- [28] K. Hajash, B. Sparrman, C. Guberan, J. Laucks, S. Tibbits, *3D Print. Addit. Manuf.* **2017**, *4*, 123.
- [29] A. K. Grosskopf, R. L. Truby, H. Kim, A. Perazzo, J. A. Lewis, H. A. Stone, *ACS Appl. Mater. Interfaces* **2018**, *10*, 23353.
- [30] W. D. Callister Jr., D. G. Rethwisch, *Materials Science and Engineering: An Introduction*, John Wiley & Sons, Inc., xxxx **2009**.
- [31] B. Goldschmidt, Best Cura Infill Pattern for Your Needs, <https://all3dp.com/2/cura-infill-patterns-all-you-need-to-know/>, (accessed: December 2021).
- [32] S.-H. Ahn, M. Montero, D. Odell, S. Roundy, P. K. Wright, *Rapid Prototypes* **2002**, *8*, 248.
- [33] J. W. Tashman, D. J. Shiwarski, A. W. Feinberg, *HardwareX* **2021**, *9*, e00170.